




THE INFLUENCE OF Fe AND Cr DOPANT IN THE SYNTHESIS OF $\text{Ca}_3\text{Co}_4\text{O}_9$ THERMOELECTRIC MATERIAL ON CRYSTAL STRUCTURE, CRYSTAL SIZE, THERMAL CONDUCTIVITY, AND ELECTRICAL CONDUCTIVITY

Imam Syafrudin Rahman¹, Rachmat Triandi Tjahjanto^{1*}, Masrurroh²

¹Department of Chemistry, Faculty of Mathematics and Natural Sciences, Brawijaya University

²Department of Physics, Faculty of Mathematics and Natural Sciences, Brawijaya University

ARTICLE INFO	ABSTRACT
<p>Keywords: <i>Calcium cobalt ($\text{Ca}_3\text{Co}_4\text{O}_9$); sol-gel; dopant; thermal conductivity; electrical conductivity.</i></p> <p><i>Article History:</i> Received: 2024-09-30 Accepted: 2024-12-01 Published: 2024-12-25 doi:10.20961/jkpk.v9i3.93818</p>  <p>© 2024 The Authors. This open-access article is distributed under a (CC-BY-SA License)</p>	<p>In this work, we study, by sol-gel method, CCO doped with Fe and Cr dopants, the implications for the aspects, crystal structure, crystal size, thermal conductivity, and electrical conductivity. Nevertheless, CCO has low thermoelectric efficiency and thus still longs for optimization in response to the performance, stability, and ecological environment requirement, which needs improvement. Dope would enhance the concentration of charge carriers without modifying the material structure itself. X-ray diffraction (XRD) to characterize the crystal structure and the Williamson–Hall (WH) method to calculate the crystal size were performed. SEM-EDS analyses provide surface morphology, particle size distribution, and elemental composition. The results show that the dopants change, among others, crystal size, microstrain, crystallinity index, and thermal and electrical conductivity, but no change in the crystal structure itself for any of these dopants. Fe doping increased the crystal size of CCO to 144.816 nm (versus 143.382 nm for pure CCO). Compared to Cr doping, the crystal's size was reduced to 65.232 nm. Where the estimated thermal conductivity increased for both dopants, attaining a value of 1.985967 W/mK for CCO-Fe and 1.952233 W/mK for CCO-Cr, concerning the value of 1.740633 W/mK of undoped CCO. Electrical conductivity also expanded (14.50 S/cm for CCO; 14.67 S/cm for CCO-Fe; 14.83 S/cm for CCO-Cr). These improvements highlight the potency of Fe and Cr dopants to fine-tune the CCO for thermoelectric usage.</p>
<p>*Corresponding Author: rachmat_t@ub.ac.id How to cite: I. S. Rahman, R. T. Tjahjanto, and Masrurroh, "The Influence of Fe and Cr Dopant in the Synthesis of $\text{Ca}_3\text{Co}_4\text{O}_9$ Thermoelectric Material on Crystal Structure, Crystal Size, Thermal Conductivity, and Electrical Conductivity," <i>J. Kim. Pendidik. Kim.</i>, vol. 9, no. 3, pp. 471-483 2024. [Online]. Available: http://dx.doi.org/10.20961/jkpk.v9i3.93818.</p>	

INTRODUCTION

Experts have been innovating different ways to access a new sustainable energy source due to the ongoing energy crisis and global pollution [1]. Among the new energy sources that have been studied are thermoelectric materials, which are materials that can convert heat energy directly into electrical energy [2]. Thermoelectric

materials are semiconductive that reversibly convert heat energy into electrical energy based on the Seebeck Effect [3]. They are efficient, durable, and have a very low environmental impact. Additionally, they can generate energy for both short-term and long-term applications. The thermoelectric figure of merit, which measures the efficiency of thermoelectric materials, is a function of the

thermal and electrical conductivity values. Thermoelectric materials are promising materials that can directly convert waste heat to electrical energy to develop sustainable energy sources. For example, various car accessories can be powered up using the heat generated by vehicle engines, reducing greenhouse gases and fossil fuel usage. Examples of thermoelectric materials include Bi_2Te_3 , Sb_2Te_3 , and $\text{BiCuSeO} \cdot \text{Ca}_3\text{Co}_4\text{O}_9$ (CCO) is one of the thermoelectric materials with very high stability and relatively good thermoelectric properties [4].

CCO has a layered structure [5] formed as polycrystalline particles. The CCO crystal structure comprises two crystal subsystems: the CoO_2 and Ca_2CoO_3 crystal systems [6]. CoO_2 is an electrical conductor layer, and the other layer, Ca_2CoO_3 , is the insulator layer. CCO has a high Seebeck coefficient and thermal stability, generating great interest in its application in thermoelectric materials [4]. CCO will resist high temperatures, thus maintaining its electrical resistance in high-temperature environments [7]. CCO is a semiconductive material still under development using different synthetic techniques and material engineering. There are various ways syntheses of CCO possible, such as solid-state reactions, spark plasma sintering (SPS), hot pressing (HP), sol-gel combustion, polymer combustion, hydrothermal decomposition, and sol-gel [8], [9], [10]. The sol-gel method will yield nanometer grain sizes of CCO, have a high homogeneity, does not require high synthesis temperatures, and is easy to use [11]. Smaller crystal sizes are achieved through

sol-gel synthesis compared to the solid-state reaction method [12]. CCO synthesis via sol-gel methods usually employs calcium nitrate and cobalt nitrate as the precursors and citric acid or nitric acid as emulsifying agents in general [13]. So, in this research, CCO was synthesized using the sol-gel method.

CCO is a good thermoelectric material that can reversibly convert thermal energy into electrical energy using the Seebeck effect. CCO offers good oxidation resistance and thermal stability [14]. Low electrical conductivity limits efficiency. Consequently, effort must be directed towards enhancing the materials' conductivity. Dopant addition is a method of improving CCO performance. Since the dopant elements do not modify the CCO's crystal structure, the increased charge carriers concentration enhance the electrical conductivity, thereby improving the material's thermoelectric property [15], [16], [17]. CCO is a p-type thermoelectric (TE) material with holes as the main charge carriers. Dopant element can substitute for Ca or Co atoms in the CCO. Using dopant elements with higher positive charge than that of the element being substituted will enhance the efficiency of the thermoelectric material. If the replacing dopant element has a +3 charge, the concentration of charge carriers will increase, leading to enhanced electrical conductivity and improved thermoelectric efficiency [3].

Iron (Fe) and chromium (Cr), dopants with +3 charge, can be utilized to enhance the efficacy of CCO. This Ca-side substitution will result in a positively charged excess in the CCO. Material can modify the electronic structure, so to stabilize the excess positive

charge, the number of holes must be increased. With increasing holes, the number of charge carriers will increase, enhancing electrical conductivity and performance [17], [18]. Research on CCO synthesis in the addition of Fe and Cr dopants using the solid-state reaction method has been conducted [8], [19]. No research has been conducted on the preparation of CCO using the sol-gel method, which investigates the effect of both Fe and Cr dopants on crystal structure, crystal size, thermal conductivity, and electrical conductivity. Therefore, this research aims to investigate the influence of Fe and Cr dopant elements in the synthesis of CCO using the sol-gel method on the material's crystal structure, crystal size, thermal conductivity, and electrical conductivity. Notably, the goal is to improve the electrical conductivity of CCO.

METHODS

1. Materials and Instruments

Materials used in this research include calcium carbonate (CaCO_3 , 99%, MERCK), cobalt(II) nitrate hexahydrate ($\text{Co}(\text{NO}_3)_2 \cdot 6\text{H}_2\text{O}$, 99%, MERCK), iron(III) nitrate nonahydrate ($\text{Fe}(\text{NO}_3)_3 \cdot 9\text{H}_2\text{O}$, 99%, MERCK), chromium(III) nitrate nonahydrate ($\text{Cr}(\text{NO}_3)_3 \cdot 9\text{H}_2\text{O}$, 99%, MERCK), nitric acid (HNO_3 , analysis grade, Panreac), citric acid (99%, Panreac), and ethylene glycol (99%, Panreac). Characterization was carried out using an X-ray diffractometer (XRD) Xpert3 Powder Panalytical, Scanning Electron Microscope (SEM) FEI Quanta FEG 650, Energy Dispersive X-ray Spectroscopy (EDS) detector using Oxford Instruments - CY809 - S tester, thermal conductivity test using

Cyeyo Thermal Conductivity Tester CY809-S, and electrical resistivity test using the JG ST2258C Four Probe Resistance Tester.

2. Synthesis of $\text{Ca}_3\text{Co}_4\text{O}_9$ (CCO), $\text{Ca}_{3-x}\text{Fe}_x\text{Co}_4\text{O}_9$ (CCO- Fe_x) ($x=0.015$), and $\text{Ca}_{3-x}\text{Cr}_x\text{Co}_4\text{O}_9$ (CCO- Cr_x) ($x=0.015$)

CCO synthesis was performed using the sol-gel method with 2.4 g of calcium carbonate (CaCO_3) and 9.312 g of cobalt nitrate ($\text{Co}(\text{NO}_3)_2 \cdot 6\text{H}_2\text{O}$) in a beaker. Synthesis of CCO-Fe ($x = 0.015$) was performed by mixing 2.3868 g of calcium carbonate (CaCO_3), 9.307344 g of cobalt nitrate ($\text{Co}(\text{NO}_3)_2 \cdot 6\text{H}_2\text{O}$), and 0.04876 g of iron (III) nitrate nonahydrate ($\text{Fe}(\text{NO}_3)_3 \cdot 9\text{H}_2\text{O}$) in a beaker at room temperature. The synthesis of CCO-Cr ($x = 0.015$) was carried out by weighing 2.3871 g of calcium carbonate (CaCO_3), 9.3085 g of cobalt nitrate ($\text{Co}(\text{NO}_3)_2 \cdot 6\text{H}_2\text{O}$), and 0.0476 g of chromium(III) nitrate nonahydrate ($\text{Cr}(\text{NO}_3)_3 \cdot 9\text{H}_2\text{O}$), then mixing them in a beaker at room temperature. Subsequently, nitric acid was added dropwise to the three mixtures until a clear pink solution was obtained. Then, 10 mL of 4 M citric acid and 10 mL of ethylene glycol were added and evaporated at 363 K until a pink gel was obtained. The samples were dried for one hour at a temperature between 363 and 393 K and ground into powder form. Then, the sample was heated at a rate of $5^\circ/\text{min}$ to a temperature of 1073 K and maintained this temperature for four hours.

3. Material Characterization

The synthesized samples were characterized at room temperature using X-ray diffractometer (XRD) in Cu-K α radiation

source (0.15418 nm), a 2θ range of 10–60°, and scan speed of 0.0017 dps. The results are used to analyze the crystal structure, crystal size, and crystallinity index of CCO. The diffractograms were compared to Masset et al. [17] and the Rietveld refinement method. Rietveld refinement technique with ICSD database numbers 095439 and 151436 was used for the Ca_2CoO_3 subsystem and CoO_2 subsystem, respectively. XRD data were processed using the Williamson-Hall (WH) formula to calculate the crystals' dimensions. The elemental surface morphology and composition of CCO were analyzed using SEM-EDS at a High Voltage (HV) of 20 kV and working distance (WD) of 10 mm. Test samples for thermal conductivity and electrical resistivity were prepared by pressing the samples into cylindrical pellets and then heat-treated at 1073 K during the annealing step. The material test was performed with the Cyeyo Thermal Conductivity Tester CY809-S and JG ST2258C Four Probe Resistance Tester. The room temperature thermal conductivity test was carried out at 7 W for 10 seconds with probe model number 2. In this case, an electrical resistivity test was performed by calculating resistivity (ρ); the measured resistance field was the linear straight line arranged by the four resistance measurement probes.

RESULTS AND DISCUSSION

1. X-ray Diffraction (XRD).

Figures 1(a) and 1(b) show the XRD diffraction patterns of the experimental results and Rietveld refinement method of CCO, CCO-Fe, and CCO-Cr samples, respectively

— the 2θ and Miller Indices (hkl) comparison table detailed in Table 1. The XRD diffraction pattern results were analyzed using the Rietveld method by comparing the diffraction pattern results with ICSD database number 095439 for the Ca_2CoO_3 subsystem and number 151436 for the CoO_2 subsystem. Subsequently, the XRD results were processed and replotted using Origin software. As depicted in Figure 1(a), no difference between the XRD diffraction pattern and the Miller Indices values is observed within the three samples, and based on Figure 1(b), the XRD diffraction pattern is also not different from the experimental results using Rietveld Refinement methods.

Table 1 compares CCO, CCO-Fe, and CCO-Cr samples for Miller Indices (hkl) values. The table presents a comparison between the index values of the experimental samples obtained from XRD results, the refinement results, and the values reported by Masset et al. [20]. No major discrepancies were observed between the Miller Indices (hkl) for values obtained from the experimental results, refinement results, and the data by Masset [20]. All ten peaks in the XRD diffraction pattern of the experimental samples matched with ICSD data in both subsystems, indicating the successful synthesis of $\text{Ca}_3\text{Co}_4\text{O}_9$ in the sol-gel process. Similarly, there was no great variation in (hkl) value, representing Miller Indices in the diffraction pattern of the CCO-Fe and CCO-Cr samples concerning the CCO sample. Hence, this indicates that Fe and Cr dopants have been successfully substituted into the CCO without influencing the crystal structure of CCO.

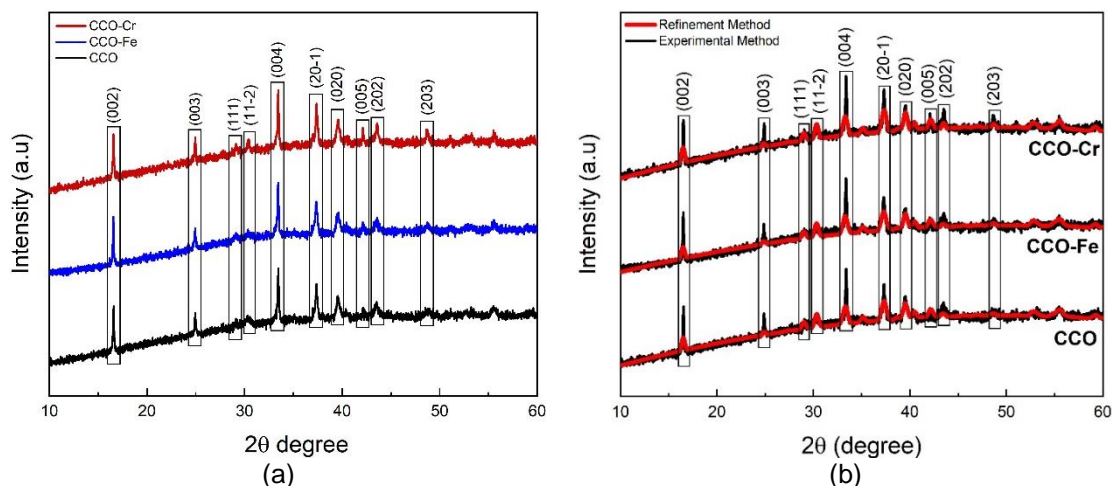


Figure 1. XRD diffraction patterns of the experimental CCO, CCO-Fe, and CCO-Cr samples (a) and XRD diffraction patterns of the CCO, CCO-Fe, and (b). CCO-Cr samples after Rietveld refinement

Table 1. Comparison of Miller index (hkl) values between Masset et al., experimental data, and refinement data for CCO, CCO-Fe, and CCO-Cr samples

hl	Masset et al., 2000	Experimental Data			Refinement Data		
		CCO	CCO-Fe	CCO-Cr	CCO	CCO-Fe	CCO-Cr
002	16.52	16.56	16.54	16.56	16.56	16.53	16.54
003	24.88	24.95	24.91	24.91	24.95	24.90	24.91
111	29.10	29.13	29.08	29.13	29.08	29.06	29.06
11-2	30.35	30.30	30.35	30.41	30.40	30.38	30.38
004	33.39	33.44	33.42	33.44	33.47	33.39	33.37
11-3	35.11	-	-	-	35.21	35.18	35.19
20-1	37.33	37.37	37.33	37.36	37.28	37.33	37.40
020	39.57	39.56	39.55	39.57	39.54	39.57	39.64
005	42.10	42.16	42.14	42.14	42.20	42.09	42.13
202	43.51	43.51	43.55	43.57	43.20	43.46	43.55
203	48.68	48.76	48.71	48.75	48.38	48.69	48.78
20-5	53.14	-	-	-	52.92	52.96	53.16

As shown in Figure 1(a), the XRD diffraction pattern of the CCO-Fe and CCO-Cr samples exhibit the same characteristic peaks as those of the CCO samples, along with their corresponding Miller Indices (hkl) values. However, shifts in the diffraction peaks are observed after substituting Fe and Cr. As shown in Table 1, diffraction peak shifting occurs at the Miller index (hkl) 00l, where a reduction of diffraction peak intensity happens. The slight shift in the diffraction peaks following Fe substitution occurs for the planes (002) (from 16.56° to 16.54°), (003) (from 24.95° to 24.91°), (004) (from 33.44° to

33.42°) and (005) (from 42.16° to 42.14°). In contrast, a shift in the diffraction peaks after Cr substitution can be observed at two distinct sites, corresponding to two Miller indices (00l): 003 (from 24.95° to 24.91°) and 005 (from 42.16° to 42.14°). The substitution of Fe and Cr into CCO can enhance thermal stability and improve electrical conductivity. Fe and Cr are dopants that modify the electronic properties, potentially stabilizing the crystal structure against phase transitions and thermal vibrations [7], [21].

2. Calculation of crystal size using the WH Plot method and sample crystallinity index

The crystal size is a calculated domain based on the characteristic of the diffraction peaks. The crystal size is different from the particle size due to the formation of polycrystalline aggregates, which consist of multiple crystal domains [22]. Lattice strain is a measure of the spread of lattice constants due to crystal structure defects, such as crystal dislocation [23]. Peak broadening in XRD diffraction patterns can be evaluated to calculate crystal size and mislocalization-induced lattice strain [24]. One of the simplest methods that can be used to calculate crystal size (t), lattice strain (ϵ), etc., is the Williamson-Hall (WH) method [25]. This approach can be expressed with the following:

$$\beta_{total} = \beta_{strain} + \beta_{size} \quad (1)$$

$$\beta_{strain} = 4\epsilon \cdot \tan\theta \quad (2)$$

$$\beta_{hkl} = (k\lambda D \cos\theta) + 4\epsilon \cdot \tan\theta \quad (3)$$

$$\beta_{hkl} \cdot \cos\theta = (k\lambda D) + 4\epsilon \cdot \tan\theta \quad (4)$$

The large crystal size and lattice strain values obtained from preceding calculations facilitate the calculation of the crystallinity index using equation (4). The formula of the crystallinity index is expressed as:

$$CI = \frac{A_{cr}}{A_{cr} + A_{amp}} \quad (5)$$

where A_{cr} refers to the area of the crystalline peaks formed, and A_{amp} refers to the total area of the amorphous peaks formed. The results of the calculations and comparisons of crystal size, microstrain, and crystallinity for the CCO, CCO-Fe, and CCO-Cr samples are shown in [Table 2](#). Based on the table, it can be seen that there is a change

in the crystal size, microstrain, and crystallinity index of CCO after being substituted by dopant. This indicates that Fe and Cr dopants affect the crystal size, lattice strain, and crystallinity index of CCO.

Although the crystal structure remains unchanged, the CCO crystal size increases by 1.434 nm to 144.816 nm after being substituted by Fe a but decreases by 78.152 nm to 65.232 nm after substitution with Cr. After Fe and Cr doping, the microstrain of CCO converts from 3.44 to 4.05 of CCO-Fe and 2.08 of CCO-Cr. The crystallinity index of CCO also varies by the substitution of Fe and Cr atoms, where the crystallinity indices of CCO, CCO-Fe, and CCO-Cr are 54%, 51.65%, and 50.15%, respectively. The XRD data in this study have values that are significantly different from previous research which has been carried out by Firdausi et al., [26] CCO calcined with a heating rate of 5°/min has a crystal size of 524.761 nm, lattice strain of 3.07, and crystallinity index of 79.31%. The results of this study demonstrate a lower crystal size, higher lattice strain, and lower crystallinity index.

The formation of larger conductive grains suggests that it improves the material's conductivity. Fewer grain boundaries are common with larger crystal sizes. There will be fewer grain boundaries through which scatter charge carriers, leading to increased electrical conductivity [27], [28]. Micro strain in CCO can lead to lattice distortion. This lattice distortion could inhibit the movement of charge carriers in the thermoelectric material. It is also observed that micro strain decreases but lattice ordering increases, ultimately improving the charge carrier

mobility and increasing the electrical conductivity [27]. A higher crystalline index value indicates a greater degree of structure

ordering which enhances charge carrier mobility and, hence, improves the electrical conductivity of the material [29].

Table 2. Comparison of crystal size, microstrain, and crystallinity of CCO, CCO-Fe, and CCO-Cr samples

Samples	Crystallite Size (nm)	Micro Strain	R ²	CI (%)
CCO	143.382	3.44	0.92996	54.00%
CCO-Fe	144.816	4.05	0.91522	51.65%
CCO-Cr	65.232	2.08	0.99059	50.15%

Grain boundaries are less frequent in greater crystal sizes. A reduced number of grain boundaries can decrease the scattering of charge carriers and potentially enhance the electrical conductivity [27], [28]. The high microstrain in CCO may lead to lattice distortion, obstructing the transport of thermoelectric charge carriers [28], [29]. Lower microstrain indicates a more orderly lattice structure, which enhances charge carrier mobility and, hence, improves electrical conductivity. As the crystallinity index value increases, the lattice structure becomes more orderly, enhancing charge carrier mobilities and potentially increasing the material's electrical conductivity [27], [29].

3. Scanning Electron Microscope-Energy Dispersive X-ray Spectroscopy (SEM-EDS)

Figure 2 displays the Scanning Electron Microscope (SEM) images and particle size distribution graphs of the CCO, CCO-Fe, and CCO-Cr samples. Figures 2 (a-c) show the morphology of CCO, which is plate-like and rounded. The CCO and CCO doped with Fe and Cr show no morphological

difference. Next, as shown in Figures 2 (d-f), each specimen's particle size distribution differs. Replacing with Fe and Cr Dopant, CCO is found to reduce the particle size distribution. Specifically, the average particle size distribution of the undoped CCO was 0.879 μm , while the CCO-Fe material exhibited an average of 0.782 μm . The CCO-Cr material had the most minor average particle size distribution of all, only 0.759 μm , thus confirming that the dopants Fe and Cr decrease the particle size distribution of the CCO.

It is assumed that a small particle size distribution would influence the material's electrical conductivity. Moreover, the contact area between particles become smaller when larger particle sizes are used compared to smaller ones. This is likely to impair the connectivity between the particles, adversely affecting the material's electrical conductivity. In contrast, decreasing the particle size allows the small particles to enter the spaces between particles, increasing the overall contact surface area and improving the electrical conductivity of the material.

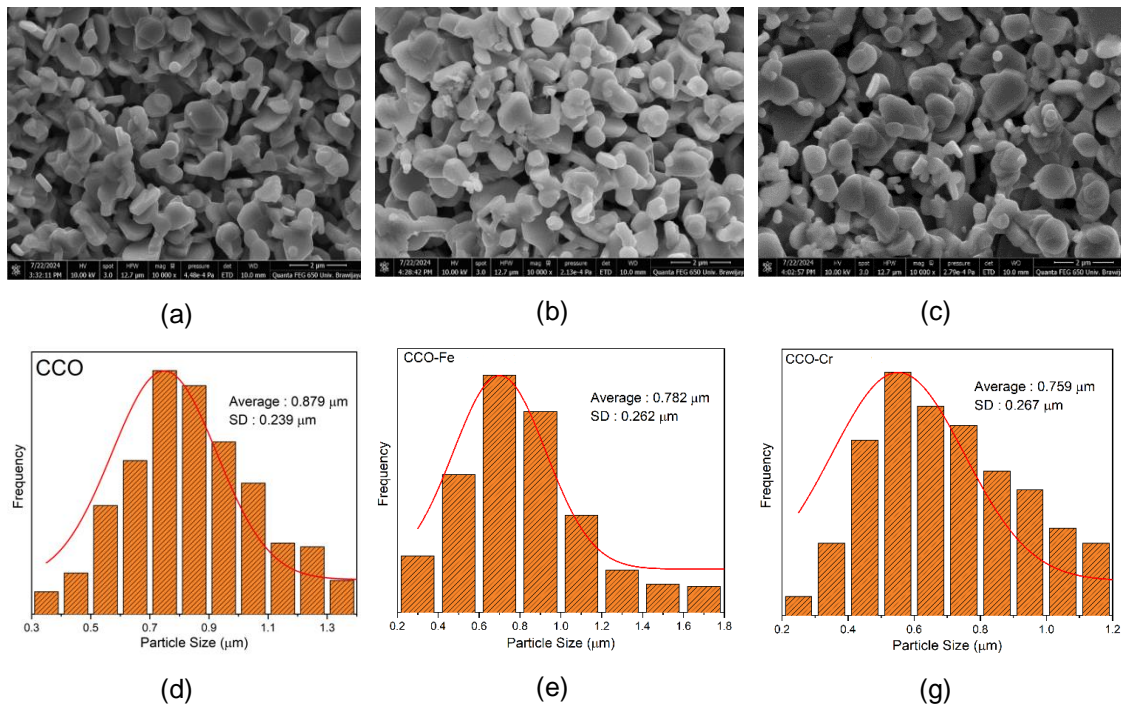


Figure 2. SEM images of CCO, CCO-Fe, and CCO-Cr samples (a-c) and particle size distribution of CCO, CCO-Fe, and CCO-Cr samples (e-g).

Table 3. Composition table of %mass and %atom for each element from SEM-EDS results of CCO, CCO-Fe, and CCO-Cr samples.

Samples	Element	%Weight	%Atom	Ratio
CCO	Ca	23.30	17.49	3
	Co	45.45	23.30	4
	O	31.35	59.21	10.16
CCO-Fe	Ca	23.00	17.28	2.992
	Co	45.22	23.10	4
	O	31.64	59.55	10.31
	Fe	0.13	0.07	0.012
CCO-Cr	Ca	21.94	16.71	2.750
	Co	46.91	24.30	4
	O	30.82	56.80	9.34
	Cr	0.33	0.19	0.031

Table 3 displays each element's mass and atomic percentages derived from EDS results. As observed in the table, there are three elements in the CCO sample and four in the CCO-Fe and CCO-Cr samples. Four Elements of CCO-Fe: The Ca:Co:O:Fe ratio is 2.992:4:10.31:0.012. These results imply that the x value for Fe dopant substitution is less than in the theoretical value (x = 0.015). Crystal lattice distortion is suspected to be responsible for the much lower Fe content

observed compared to the theoretical value [27], which causes the incorporation of Fe into the lattice to become less effective. The CCO-Cr sample also contains four elements with a Ca:Co:O:Cr ratio of 2.750:4:9.34:0.031. This ratio behaves differently compared to Fe doping as the Cr dopant substitution is higher than the theoretical value (x = 0.015). The substitution of Cr dopant greatly surpasses the theoretical value, approximately doubling the predicted

amount, unlike the case with Fe doping. This issue is suspected to come from the use of a Cr dopant precursor that is not accurately taken according to the desired molar amount. The precursor used was chromium(III) nitrate nonahydrate ($\text{Cr}(\text{NO}_3)_3 \cdot 9\text{H}_2\text{O}$), which is highly hygroscopic due to its high hydrate content. The dehydration of this compound can cause discrepancy in its relative molecular mass (M_r), leading to a lower than expected M_r . Lower M_r value leads to a higher molar amount of precursor, subsequently a higher amount of substituted Cr.

As indicated by the EDS results, the significant difference in the amount of Fe and Cr substituted in the CCO makes direct comparison between these two dopants impractical. As mentioned, the CCO-Cr material also has the smallest crystal size, lowest microstrain, small particle size, and highest crystallinity index among other materials. This is thought to be related to the thermal and electrical conductivity of the material, which could represent the highest or the lowest values among the samples. Therefore, the material will undergo further testing for thermal and electrical conductivity.

4. Thermal Conductivity Test (κ)

Table 4 displays the thermal conductivity test results for CCO and CCO with dopants measured thrice. It shows that the thermal conductivity of CCO (1.740633 W/mK) was increased by 0.245334 W/mK after the substitution of Fe and by 0.2116 W/mK when substituted by Cr (1.985967 W/mK + 0.2116 W/mK) (Table 4). The thermal conductivity of CCO reported by

Firdausi et al. [26] was 1.863667 W/mK, which is higher than the value of thermal conductivity of CCO in this study. Based on the conductivity data in the table, the value increases from CCO to CCO-Fe, followed by a decrease in CCO-Cr. Both dopants were incorporated into the CCO, increasing charge carriers available for the conduction process, which then change the electrical conductivity. An increase in charge carriers can also affect thermal conductivity if phonon scattering is reduced. Thus, the dopants in the CCO increases the number of charge carriers, reduces phonon scattering, and can subsequently enhance thermal conductivity [29]. We observed that the thermal conductivity of the CCO samples substituted with Fe dopants is different from that with Cr. This thermal conductivity of the CCO-Cr sample is lower than that of the CCO-Fe sample. This could be attributed to its smaller particle size distribution (0.759 μm for CCO-Cr; 0.782 μm for CCO-Fe), which promote grain boundaries. The increase in grain boundaries increases the phonon resistance and thus reduces thermal conductivity [30].

5. Electrical Resistivity Test

Table 5 shows the results of the electrical resistivity (ρ) tests for the CCO, CCO-Fe, and CCO-Cr samples after three repetitions. The electrical resistivity values for CCO, CCO-Fe, and CCO-Cr materials are 68.93, 68.13, and 67.43 $\text{m}\Omega\text{cm}$, respectively, indicating that the introduction of dopants leads to a decrease in the electrical resistivity of the material. Electrical resistivity tests conducted in previous studies [26] found that

CCO had a resistivity value of 89.23333 mΩcm, whereas this study shows a lower resistivity value for CCO. As Equation (6) mentioned, a lower electrical resistivity value means higher conductivity. The relation between electrical resistivity and electrical conductivity (σ) is expressed as follows:

$$\sigma = \frac{1}{\rho} \quad (6)$$

where ρ represents electrical resistivity ($\Omega \cdot \text{cm}$) and σ represents electrical conductivity (S/cm).

Table 4. Results of thermal conductivity (κ) tests for CCO, CCO-Fe, and CCO-Cr samples.

Samples	Repetition (W/mK)			κ (W/mK)
	1	2	3	
CCO	1.7880	1.7861	1.6478	1.740633±0.0701
CCO-Fe	2.0859	1.9287	1.9433	1.985967±0.0786
CCO-Cr	2.0787	1.8810	1.8970	1.952233±0.0988

Table 5. Results of electrical resistivity (ρ) tests for CCO, CCO-Fe, and CCO-Cr samples.

Samples	Repetition (mΩcm)			ρ (mΩcm)	σ (S/cm)
	1	2	3		
CCO	66.5	68.8	71.5	68.93333±2.5	14.507471
CCO-Fe	66.1	69.8	68.5	68.13333±1.85	14.677104
CCO-Cr	65.8	69.6	66.9	67.43333±1.9	14.829468

The +3 charged dopants Fe and Cr replace +2 charged Ca. When Fe and Cr are doped to the material, there is a surplus of positive charge. The material has to enhance the number of positive charge carriers, known as holes in the CCO, to preserve this surplus positive charge. The electrical conductivity of the CCO increases with the number of holes [18]. A direct comparison cannot be made since the concentrations for the Fe and Cr dopants differ according to the EDS results. Figure 3 presents the comparison graphs of thermal and electrical conductivity for the CCO, CCO-Fe, and CCO-Cr materials. However, electrical conductivity depends on temperature. At high dopant concentrations, structural distortions may hinder charge carrier mobility, which can reduce conductivity [18].

As shown in Table 5, the electrical conductivity values derived from resistance measurements were 14.50, 14.67, and 14.82 S/cm for CCO, CCO-Fe, and CCO-Cr, respectively. The conductivity increased from 14.50 to 14.67 S/cm with Fe substitution (an increased of 0.17 S/cm) and increased to 14.82 S/cm with Cr substitution (an increased of 0.32 S/cm). Crystal size can provide information about the change in electrical conductivity due to dopants. Substitution with Fe will increase the electrical conductivity by about 0.17 S/cm and increase the crystal size by about 1.434 nm. Conversely, Cr substitution reduces the crystal size by 78.152 nm which improves the conductivity to 0.32 S/cm. Relative to previous studies [8], [19], [31] that examined only a single dopant type (Fe or Cr) on the thermoelectric properties of $\text{Ca}_3\text{Co}_4\text{O}_9$, no study has

explored the influence of dopants on crystal sizes, microstrain, crystallinity index, thermal conductivity, and electrical conductivity. This study, therefore, presents a comparative studies of CCO substituted with two different dopants and investigates their effects on crystallite size, lattice strain, crystallinity index, thermal conductivity, and electrical conductivity and the correlation among parameters.

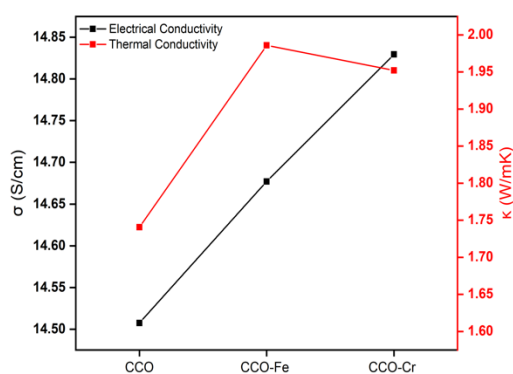


Figure 3. Comparison curve between thermal conductivity and electrical conductivity of the samples.

CONCLUSION

The $\text{Ca}_3\text{Co}_4\text{O}_9$ material was successfully synthesized using the sol-gel method with the addition of Fe and Cr dopants. Adding Fe and Cr dopants did not significantly change the crystal structure of CCO. No variation was observed in the XRD diffraction pattern or the Miller indices of the CCO due to the substituted dopants, as seen in the XRD analysis results. It should be noted that the amount of dopants used for Fe and Cr is significantly different, so each dopant's effect cannot be directly compared. Crystal size, lattice strain, crystallinity index, thermal conductivity, and electrical

conductivity of CCO can all be affected by the incorporation of Fe and Cr dopants. After doping with Fe and Cr, the electrical conductivity of CCO increased greatly, and the electrical conductivity was 14.83 for CCO-Cr, 14.67 for CCO-Fe, and 14.50 for CCO. According to this study, it was demonstrated that the electrical conductivity of CCO was improved with Fe and Cr as dopant substitution. However, in this work, the dopant concentration optimization work to improve the electrical conductivity of CCO has not been done. Hence, future investigations could explore variations in dopant concentrations in CCO to achieve optimal performance. This study in this field aims to identify a minimal and energy-efficient thermoelectric material by optimizing both temperature and chemical composition in $\text{Ca}_3\text{Co}_4\text{O}_9$, while considering the high costs and environmental sustainability for commercial competitiveness.

ACKNOWLEDGE

Thanks to FMIPA Universitas Brawijaya through Hibah Doktor Lektor Kepala 2024 for funding this research. Thanks also to the Laboratorium Riset Terpadu Universitas Brawijaya (LRTUB) for helping to carry out the characterizations using SEM and XRD.

REFERENCES

- [1] M. d'Angelo, C. Galassi, and N. Lecis, "Thermoelectric Materials and Applications: A Review," *Energies*, vol. 16, no. 17, p. 6409, Sep. 2023, doi: [10.3390/en16176409](https://doi.org/10.3390/en16176409).
- [2] D. Thomazini, A. Dos Santos Lima, and M. V. Gelfuso, "Synthesis and characterization of cold sintered

- Ca₃Co₄O₉ ceramics obtained by a simplified Pechini route," *Mater. Today Commun.*, vol. 35, p. 105887, Jun. 2023, doi: [10.1016/j.mtcomm.2023.105887](https://doi.org/10.1016/j.mtcomm.2023.105887).
- [3] J. Fang, H. Yang, L. Liu, Q. Kang, and Y. Gou, "Research progress on doping modification of Ca₃Co₄O₉ thermoelectric materials: A review," *J. Mater. Sci.*, vol. 59, no. 6, pp. 2228–2257, Feb. 2024, doi: [10.1007/s10853-024-09342-9](https://doi.org/10.1007/s10853-024-09342-9).
- [4] S. D. Yudanto, "Preparasi, Sintesis dan Karakterisasi Material Oksida Ca₃Co₄O₉," unpublished.
- [5] A. Weidenkaff et al., "Development of Perovskite-type Cobaltates and Manganates for Thermoelectric Oxide Modules," *J. Korean Ceram. Soc.*, vol. 47, no. 1, pp. 47–53, Jan. 2010, doi: [10.4191/KCERS.2010.47.1.047](https://doi.org/10.4191/KCERS.2010.47.1.047).
- [6] Y. C. Liou, W. C. Tsai, W. Y. Lin, and U. R. Lee, "Synthesis of Ca₃Co₄O₉ and CuAlO₂ Ceramics of the Thermoelectric Application Using A Reaction-Sintering Process," *J. Aust. Ceram. Soc.*, 2008.
- [7] Y. Li et al., "An electrochemically neutralized energy-assisted low-cost acid-alkaline electrolyzer for energy-saving electrolysis hydrogen generation," *J. Mater. Chem. A*, vol. 6, no. 12, pp. 4948–4954, 2018, doi: [10.1039/C7TA10374C](https://doi.org/10.1039/C7TA10374C).
- [8] F. Delorme et al., "Effect of Ca substitution by Fe on the thermoelectric properties of Ca₃Co₄O₉ ceramics," *J. Electroceram.*, vol. 40, no. 2, pp. 107–114, Apr. 2018, doi: [10.1007/s10832-018-0109-2](https://doi.org/10.1007/s10832-018-0109-2).
- [9] J. R. Rajabathar et al., "Structural and electrical property characterization of thermoelectric (Ca₃Co₄O₉±δ) ceramic oxide fabrication by various reducing agent method," *J. Mater. Sci. Mater. Electron.*, vol. 34, no. 7, p. 585, Mar. 2023, doi: [10.1007/s10854-023-09986-4](https://doi.org/10.1007/s10854-023-09986-4).
- [10] S. Katsuyama et al., "Synthesis of Ca₃Co₄O₉ ceramics by polymerized complex and hydrothermal hot-pressing processes and the investigation of its thermoelectric properties," *J. Mater. Sci.*, vol. 43, no. 10, pp. 3553–3559, May 2008, doi: [10.1007/s10853-008-2561-x](https://doi.org/10.1007/s10853-008-2561-x).
- [11] S. D. Yudanto et al., "Sintesis dan Karakterisasi Keramik Ca₃Co₄O₉ Melalui Metode Sol-Gel," vol. 30, no. 1, 2021, unpublished.
- [12] A. K. Królicka et al., "Effect of sol-gel and solid-state synthesis techniques on the structural, morphological and thermoelectric performance of Ca₃Co₄O₉," *Ceram. Int.*, vol. 44, no. 12, pp. 13736–13743, Aug. 2018, doi: [10.1016/j.ceramint.2018.04.215](https://doi.org/10.1016/j.ceramint.2018.04.215).
- [13] J. Mastalska-Popławska et al., "Role of starch in the ceramic powder synthesis: A review," *J. Sol-Gel Sci. Technol.*, vol. 96, no. 3, pp. 511–520, Dec. 2020, doi: [10.1007/s10971-020-05404-x](https://doi.org/10.1007/s10971-020-05404-x).
- [14] A. Bhaskar et al., "Thermoelectric Properties of Ca_{3-x}DyxCo₄O_{9+δ} with x = 0.00, 0.02, 0.05, and 0.10," *J. Electron. Mater.*, vol. 42, no. 8, pp. 2582–2586, Aug. 2013, doi: [10.1007/s11664-013-2634-8](https://doi.org/10.1007/s11664-013-2634-8).
- [15] C.-J. Liu et al., "Improvement of the thermoelectric characteristics of Fe-doped misfit-layered Ca₃Co_{4-x}Fe_xO_{9+δ} (x=, 0.05, 0.1, and 0.2)," *Appl. Phys. Lett.*, vol. 89, no. 20, p. 204102, Nov. 2006, doi: [10.1063/1.2390666](https://doi.org/10.1063/1.2390666).
- [16] S. Butt et al., "Enhancement of thermoelectric performance in Cd-doped Ca₃Co₄O₉ via spin entropy, defect chemistry, and phonon scattering," *J. Mater. Chem. A*, vol. 2, no. 45, pp. 19479–19487, Oct. 2014, doi: [10.1039/C4TA03891F](https://doi.org/10.1039/C4TA03891F).
- [17] S. W. Nam et al., "Improvement in High-Temperature Thermoelectric Properties

- by Adding Mn for Co in Ca₃Co₄O₉," *J. Nanosci. Nanotechnol.*, vol. 10, no. 11, pp. 7689–7693, Nov. 2010, doi: [10.1166/jnn.2010.2784](https://doi.org/10.1166/jnn.2010.2784).
- [18] G. Constantinescu et al., "Prospects for Electrical Performance Tuning in Ca₃Co₄O₉ Materials by Metallic Fe and Ni Particles Additions," *Materials*, vol. 14, no. 4, p. 980, Feb. 2021, doi: [10.3390/ma14040980](https://doi.org/10.3390/ma14040980).
- [19] Y. Huang et al., "Enhanced Thermoelectric Performance Induced by Cr Doping at Ca-Sites in Ca₃Co₄O₉ System," *J. Am. Ceram. Soc.*, vol. 97, no. 11, pp. 3589–3596, Nov. 2014, doi: [10.1111/jace.13144](https://doi.org/10.1111/jace.13144).
- [20] A. C. Masset et al., "Misfit-layered cobaltite with an anisotropic giant magnetoresistance: Ca₃Co₄O₉," *Phys. Rev. B*, vol. 62, no. 1, p. 166, 2000, doi: [10.1103/PhysRevB.62.166](https://doi.org/10.1103/PhysRevB.62.166).
- [21] R. Higler and J. Sprakel, "Doping colloidal bcc crystals — interstitial solids and meta-stable clusters," *Sci. Rep.*, vol. 7, no. 1, p. 12634, Oct. 2017, doi: [10.1038/s41598-017-12730-8](https://doi.org/10.1038/s41598-017-12730-8).
- [22] K. Ramakanth, *Basics of Diffraction and Its Application*. New Delhi: International Publishing House Pvt. Ltd., 2007.
- [23] Y. F. Zhang et al., "Synthesis and characterization of Ca₃Co₄O₉ nanoparticles by citrate sol-gel method," *Mater. Lett.*, vol. 60, no. 20, pp. 2443–2446, Sep. 2006, doi: [10.1016/j.matlet.2006.01.013](https://doi.org/10.1016/j.matlet.2006.01.013).
- [24] R. Yogamalar et al., "X-ray peak broadening analysis in ZnO nanoparticles," *Solid State Commun.*, vol. 149, no. 43, pp. 1919–1923, 2009.
- [25] C. U. Nikam et al., "Williamson-Hall and Size-strain plot based micro-structural analysis and evaluation of elastic properties of Dy³⁺ substituted Co-Zn nano-spinels," *J. Phys. Conf. Ser.*, vol. 2426, no. 1, p. 012029, Feb. 2023, doi: [10.1088/1742-6596/2426/1/012029](https://doi.org/10.1088/1742-6596/2426/1/012029).
- [26] S. Firdausi et al., "The effect of heating rate on the thermal and electrical conductivity of Ca₃Co₄O₉ as a thermoelectric material," *Mater. Res. Innov.*, pp. 1–8, May 2024, doi: [10.1080/14328917.2024.2354078](https://doi.org/10.1080/14328917.2024.2354078).
- [27] G. Constantinescu et al., "Effect of Na doping on the Ca₃Co₄O₉ thermoelectric performance," *Ceram. Int.*, vol. 41, no. 9, pp. 10897–10903, Nov. 2015, doi: [10.1016/j.ceramint.2015.05.031](https://doi.org/10.1016/j.ceramint.2015.05.031).
- [28] T. Okuyama et al., "Synthesis and characterization of Ca₃Co₄O₉ thermoelectric ceramics using the slurry sintering method," *Electron. Commun. Jpn.*, vol. 102, no. 1, pp. 3–9, Jan. 2019, doi: [10.1002/ecj.12129](https://doi.org/10.1002/ecj.12129).
- [29] T. Wu et al., "On the origin of enhanced thermoelectricity in Fe doped Ca₃Co₄O₉," *J. Mater. Chem. C*, vol. 1, no. 26, p. 4114, 2013, doi: [10.1039/c3tc30481g](https://doi.org/10.1039/c3tc30481g).
- [30] J. Torres, "Significant enhancement of the thermoelectric performance in Ca₃Co₄O₉ thermoelectric materials through combined strontium substitution and hot pressing process," unpublished.
- [31] A. J. M. Lima et al., "Fe-doped calcium cobaltites as electrocatalysts for oxygen evolution reaction," *Ceram. Int.*, vol. 47, no. 18, pp. 26109–26118, Sep. 2021, doi: [10.1016/j.ceramint.2021.06.01731](https://doi.org/10.1016/j.ceramint.2021.06.01731).